The Canadian Mineralogist
Vol. 57, pp. 371-382 (2019)
DOI: 10.3749/canmin.1800081

CATION ORDER IN THE CRYSTAL STRUCTURE OF 'Ca-HINGGANITE-(Y)'

MARK A. COOPER AND FRANK C. HAWTHORNE[§]

Department of Geological Sciences, University of Manitoba, Winnipeg, Manitoba, R3T 2N2, Canada

RITSURO MIYAWAKI

Department of Geology and Paleontology, National Museum of Nature and Science, 4-1-1 Amakubo, Tsukuba 305-0005, Japan

ROY KRISTIANSEN

PO Box 32, N-1650, Sellebakk, Norway

ABSTRACT

The crystal structure of 'Ca-hingganite-(Y)', triclinic *P*1, *a* 9.863(4), *b* 7.602(3), *c* 4.762(2) Å, α 90.002(15), β 90.073(7), γ 90.020(5)°, *V* 357.1(5) Å^3, $Z = 1$, has been refined to an R_1 index of 2.28% for 4186 observed ($|F_o| > 4\sigma F$) reflections. Significant observed ($|F_o| > 20$–$50\ \sigma F$) reflections violate the presence of a 2_1-screw axis and an *a*-glide plane, negating the space group $P2_1/a$ previously found for minerals of the gadolinite supergroup. Averaging of the X-ray data in Laue groups 2/*m* and $\bar{1}$ gives the agreement indices 2/*m* (2.90%) and $\bar{1}$ (2.61%). The internal agreement index from averaging of identical reflections collected at multiple positions along the diffraction vector (R_{psi}) is 2.12%, where 13,801 reflections were collected, 4204 are unique for *P*1 symmetry, and R_{psi} is based on a mean data-redundancy factor of >3. The $|E^2 - 1|$ value of 0.783 is in agreement with *P*1 as the correct space group. The general formula for the gadolinite supergroup is $A_2MQ_2T_2O_8\varphi_2$ ($Z = 2$), which we have expanded to 20 anions ($Z = 1$) to show the *A*-site cation ordering present in 'Ca-hingganite-(Y)'. Ca and Y(Ln) are ordered over four *A* sites: Y(Ln) is dominant at *A*1 [= 0.90 Y + 0.07 Er + 0.03 Ca], Ca is dominant at *A*2 [= 0.92 Ca + 0.08 Y], and there is near-equal Ca and Y(Ln) at *A*3 [= 0.55 Ca + 0.42 Y + 0.03 Er] and *A*4 [= 0.50 Ca + 0.47 Y + 0.03 Er]. The resulting site-specific empirical formula is $^{A}(Ca_{2.021}Y_{1.811}Ln_{0.133})_{\Sigma 3.965}{}^{M}(\square_{1.191}Fe_{0.794}Mn_{0.009}Mg_{0.006})_{\Sigma 2}{}^{Q}(Be_{2.24}B_{1.58}Si_{0.224})_{\Sigma 4.044}{}^{T}Si_4O_{16}{}^{\varphi}[(OH)_{2.382}O_{1.618}]_{\Sigma 4}$. The dominant constituent at the *M* site is vacancy, and Ca does not occur at the *M* site. Significant B and Si are assigned to the Be-dominant *Q* sites, and the *T* sites are occupied by Si. The simplified formula for 'Ca-hingganite-(Y)' ($Z = 1$) is $^{A}[(Y,Ln)Ca(Y,Ca,Ln)_2]^{M}(\square,Fe)_2{}^{Q}(Be,B,Si)_4{}^{T}Si_4O_{16}[(OH),O]_4$.

Keywords: 'Ca-hingganite-(Y)', crystal structure, *P*1 symmetry, cation order, gadolinite supergroup, gadolinite subgroup.

INTRODUCTION

The minerals of the gadolinite supergroup have the general formula $A_2MQ_2T_2O_8\varphi_2$ (Bačík *et al*. 2017) where A = Ca, REE (Y + lanthanides), actinoids, Pb, Mn^{2+}, Bi; M = Fe, □ (vacancy), Mg, Mn, Zn, Cu, Al; Q = B, Be, Li; T = Si, P, As, B, Be, S; φ = O, OH, F. The gadolinite supergroup is divided into two groups according to the prevailing cation-charge at the *T* site: Si^{4+} in the gadolinite group and P^{5+} or As^{5+} in the herderite group. The gadolinite group is divided into the gadolinite and datolite subgroups. In the datolite subgroup, the *A* site is occupied dominantly by divalent cations, whereas in the gadolinite subgroup, the *A* site is occupied dominantly by trivalent cations. In turn, the *Q* site is occupied dominantly by B^{3+} in the datolite subgroup and by Be^{2+} in the gadolinite subgroup (Bačík *et al*. 2017).

Minasgeraisite-(Y), endmember formula $Y_2CaBe_2Si_2O_{10}$, and hingganite-(Y), endmember formula $Y_2\square Be_2Si_2O_8(OH)_2$, are assigned to the gadolinite subgroup (Be dominant at the *Z* site) as A = Y and Q

§ *Corresponding author e-mail address*: frank_hawthorne@umanitoba.ca

= Be. Minasgeraisite-(Y) is the only member of this group with Ca assigned to the octahedrally coordinated *M* site, which has been of some concern as Ca is generally assigned to the larger [8]-coordinated *A* site in other members of the group (*e.g.*, Demartin *et al.* 2001, Bačík *et al.* 2014). The orientation of the unit cell of the gadolinite supergroup structure has fluctuated in the past: the review by Bačík *et al.* (2014) used the $P2_1/a$ setting, and the original description of minasgeraisite-(Y) (Foord *et al.* 1986) also used the $P2_1/a$ setting; on the other hand, the nomenclature paper of the gadolinite supergroup used the $P2_1/c$ setting. Here we will use the $P2_1/a$ setting, as this has the advantage that the sheets of tetrahedra in the structure stack along the **c** axis, as is commonly the case for sheet-silicate minerals.

A recent structure determination of the crystal structure of 'minasgeraisite-(Y)' (Cooper & Hawthorne 2018) showed that the structure is actually triclinic: space group *P*1. This result prompted investigation of the structure of hingganite-(Y) (this work) and again we found that the resulting structure is triclinic: space group *P*1. As noted by Cooper & Hawthorne (2018) and Miyawaki *et al.* (2018), this difference in symmetry affects the nomenclature and classification of the minerals of the gadolinite supergroup in general and the gadolinite subgroup in particular. The triclinic nature of these structures results in strong order of cations over sites (in space group *P*1) that are equivalent in the space group $P2_1/a$ and can potentially lead to new species. However, the naming of such species is better left to a more general consideration of the structures of the gadolinite-supergroup minerals. Thus, rather than assign a formal name to the material from the Heftetjern granitic pegmatite, Norway, described here, we will write the name as 'Ca-hingganite-(Y)', the single quotation marks (inverted commas) indicating that we are not implying that the material is hingganite-(Y) and the prefix Ca- indicating that, unlike hingganite-(Y), 'Ca-hingganite-(Y)' has *A*-group cations of ~50% Ca.

Occurrence

The mineral occurs in the Heftetjern granitic pegmatite, located in southern Norway at 59°8.6′N, 8°45.4′E, about 4.8 km NW of the small parish of Tørdal at an altitude of *ca.* 650 m above sea level. It is the type locality of oftedalite, kristiansenite, heftetjernite, and agakhanovite-(Y). The pegmatite consists dominantly of cleavelandite, partly amazonitic microcline, quartz, and dark and light mica, with minor oligoclase. Primary accessory minerals include beryl, spessartine, gadolinite-(Y), cassiterite, Sc-rich ixiolite, scandium-bearing pyrochlore-group minerals, and milarite. A late mineral assemblage encountered mainly in vugs and fractures comprises bertrandite, bohseite, bazzite, Sc-rich helvite, cascandite, scandiobabingtonite, and thortveitite. The numerous granite pegmatites of the Tørdal area are situated within the Nissedal volcano sedimentary outlier. Both the outlier (1300–1200 Ma) and older basement (1520–1500 Ma) are intruded by the Tørdal granite (960–850 Ma), which is regarded as the source of the pegmatite swarms. For further details, consult Cooper *et al.* (2006) and Miyawaki *et al.* (2015).

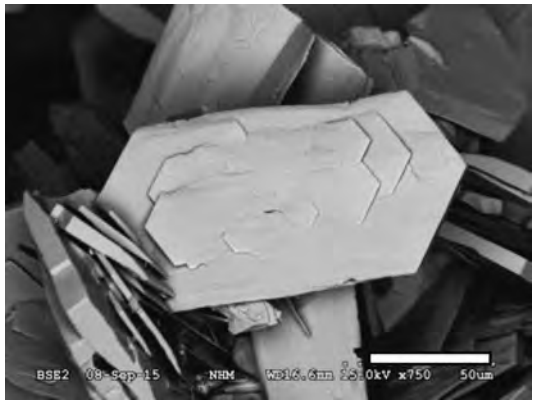

FIG. 1. SEM image of crystals of 'Ca-hingganite-(Y)' from the Heftetjern granitic pegmatite.

Individual crystals of 'Ca-hingganite-(Y)' occur as colorless or pale-yellow transparent thin pseudo-hexagonal plates up to 200 μm across (Fig. 1), as intergrown aggregates or clusters up to 1 cm across with hundreds of crystals in voids in feldspar. Associated minerals are Ce- and Sc-rich epidote, bertrandite, spessartine, occasional Mn-bearing hellandite-(Y) (Miyawaki *et al.* 2015), and Y-rich fluorite. 'Ca-hingganite-(Y)' is of late hydrothermal origin and formed in vugs in feldspar and quartz, probably after a primary beryllium mineral (perhaps gadolinite). A characteristic feature of the pegmatite is the extensive assemblage of Be and Sc minerals, with 16 Be-minerals and nine Sc minerals.

Chemical Composition

Following collection of the X-ray diffraction data, the 'Ca-hingganite-(Y)' crystal was attached to the surface of a plexiglass disk, immersed in room temperature-curing epoxy, and polished. As the starting thickness of the crystal was only 10 microns, extreme care in polishing was taken to maximize the final thickness of the polished crystal. The chemical composition was determined using a JEOL 8800M electron microprobe (WDS mode, 15 kV, 20 nA, and 2 μm beam diameter) with the following standards: wollastonite for Ca and Si, rhodonite for Mn,

TABLE 1. CHEMICAL DATA FOR 'Ca-HINGGANITE-(Y)'

	wt.%	Range		*apfu*
CaO	14.02	13.62–14.31	Ca^{2+}	2.021
Y_2O_3	25.30	24.29–26.39	Y^{3+}	1.811
La_2O_3	0.05	0.00–0.11	La^{3+}	0.002
Ce_2O_3	0.08	0.00–0.20	Ce^{3+}	0.004
Pr_2O_3	0.05	0.00–0.30	Pr^{3+}	0.002
Nd_2O_3	0.12	0.08–0.23	Nd^{3+}	0.006
Sm_2O_3	0.05	0.00–0.23	Sm^{3+}	0.002
Gd_2O_3	0.13	0.05–0.29	Gd^{3+}	0.006
Tb_2O_3	0.03	0.00–0.18	Tb^{3+}	0.001
Dy_2O_3	0.19	0.07–0.27	Dy^{3+}	0.008
Ho_2O_3	0.08	0.00–0.29	Ho^{3+}	0.003
Er_2O_3	0.41	0.13–0.54	Er^{3+}	0.017
Tm_2O_3	0.12	0.00–0.23	Tm^{3+}	0.005
Yb_2O_3	1.52	1.22–1.78	Yb^{3+}	0.062
Lu_2O_3	0.31	0.14–0.48	Lu^{3+}	0.013
ThO_2	0.06	0.00–0.17	Th^{4+}	0.002
FeO	7.06	6.83–7.40	Fe^{2+}	0.794
MnO	0.08	0.04–0.14	Mn^{2+}	0.009
MgO	0.03	0.01–0.05	Mg^{2+}	0.006
SiO_2	31.40	30.91–31.86	Si^{4+}	4.224
BeO*	6.93		Be^{2+}	2.24
B_2O_3*	6.80†		B^{3+}	1.58
H_2O**	2.65		(OH)	2.382
Total	97.47			

* Derived from structural *Q* sites
** Derived from *M*-site vacancy (Demartin *et al.* 2001)
† 6.39 EMPA data.

sillimanite for Al, fayalite for Fe, danburite for B, $REEP_5O_{14}$ for each rare earth element (Y and lanthanoids, La–Lu), ThO_2 for Th, UO_2 for U, albite for Na, and BaF_2 for F. The B$K\alpha$ analytical line was monochromatized by the LDE2 layered dispersion element on the spectrometer. The elements F, Na, and Al are below their detection limits. No other element with atomic number ≥ 5, except for C from carbon coating and O as a constituent, was detected. The average (and range) weight-percent oxide values are reported in Table 1. The data were normalized to 20 anions with the B, Be, and (OH) values derived from crystal-chemical considerations. Our usual procedure for the acquisition of electron-microprobe data for the lanthanides would be to use a 20 kV operating voltage to the electron gun; however, equipment problems limited us to 15 kV, and this may in part be reflected in the slightly low analytical total.

X-ray Data Collection

A crystal of 'Ca-hingganite-(Y)' was attached to a MiTeGen polymer loop with a minute application of vacuum grease and mounted on a Bruker D8 three-circle diffractometer equipped with a rotating-anode generator (Mo$K\alpha$), multilayer optics, and an APEX-II detector. A total of 13,801 reflections (4204 in the Ewald sphere) was collected to 60° 2θ using 6 s per 0.3° frame with a crystal-to-detector distance of 50 mm. Empirical absorption corrections (SADABS; Sheldrick 2008) were applied and identical reflections (collected at multiple positions along the diffraction vector) were corrected for Lorentz, polarization, and background effects, averaged and reduced to structure factors. The unit-cell dimensions were obtained by least-squares refinement of the positions of 4083 reflections with $I > 10\sigma I$ and are given in Table 2, together with other information pertaining to data collection and structure refinement.

Crystal-Structure Refinement

Triclinic versus monoclinic character of the single-crystal X-ray diffraction data

All crystal structure work on the minerals of the gadolinite supergroup has been done in the space

TABLE 2. MISCELLANEOUS CRYSTALLOGRAPHIC DATA FOR 'Ca-HINGGANITE-(Y)'

a (Å)	9.863(4)	Crystal size (μm)	10 × 60 × 70
b	7.602(3)	Radiation	Mo$K\alpha$
c	4.762(2)	No. of reflections	13,801
α (°)	90.002(15)	No. in Ewald sphere	4204
β	90.073(7)	R_{psi} (%)	2.12
γ	90.020(5)	No. unique reflections	4204
V (Å^3)	357.1(5)	No. with ($F_o > 4\sigma F$)	4186
Space group	*P*1	R_1 (%)	2.28
Z	1	wR_2 (%)	5.77
Primary domain	0.323	(primary domain)^{Fr}	0.318(5)
(100) twin fraction	0.164(4)	(100) (twin fraction)^{Fr}	0.195(4)

Cell content: $(Ca_{1.992}Y_{1.873}Er_{0.135})_{\Sigma 4}(\square_{1.216}Fe_{0.784})_{\Sigma 2}(Be_{2.24}B_{1.58}Si_{0.18})_{\Sigma 4}Si_4O_{16}[(OH)_{2.382}O_{1.618}]_{\Sigma 4}$

Fr = Freidel component; $R_1 = \Sigma(|F_o| - |F_c|)/\Sigma|F_o|$; $wR_2 = [\Sigma w(F^2_o - F^2_c)^2/\Sigma w(F^2_o)^2]^{½}$, $w = 1/[\sigma^2(F^2_o) + 0.0278\ P)^2 + 0.79\ P]$, where $P = (\max(F^2_o,0) + 2F^2_c)/3$.

group $P2_1/a$ (or $P2_1/c$ setting), except for 'minasgeraisite-(Y)' which was refined in $P1$ (Cooper & Hawthorne 2018). As with 'minasgeraisite-(Y)', the X-ray data for our 'Ca-hingganite-(Y)' includes very significant intensity ($|F_o| > 20$–$50\ \sigma|F|$) for reflections that violate both the presence of a 2_1-screw axis ($0k0$; $k = 2n$) and an a-glide plane ($h00$, $h0l$; $h = 2n$). These violating reflections are also clearly observed on precession slices constructed from the raw data frames [as was the case for 'minasgeraisite-(Y)']. Our refined unit-cell parameters are compatible with both monoclinic and triclinic symmetry, as our unconstrained α and γ angles deviate $\leq 0.05°$ from 90°. These same characteristics (*i.e.*, $P2_1/a$ space group violations, monoclinic cell-metrics) were also observed for 'minasgeraisite-(Y)' (Cooper & Hawthorne 2018). Next we investigated the merging of potentially equivalent reflections for the space groups $P2_1/a$, $P\overline{1}$, and $P1$. The corrected X-ray intensity file contains 13,801 intensities which combine to give 4204 reflections in the Ewald sphere; thus there is a mean redundancy factor slightly in excess of ×3 for individual reflections. For $P2_1/a$ symmetry, there are 1055 unique reflections with $R_{merge}(sigma) = 2.90(1.07)\%$; for $P\overline{1}$ symmetry, there are 2111 unique reflections with $R_{merge}(sigma) = 2.61(1.45)\%$; for $P1$ symmetry, there are 4204 unique reflections with $R_{psi}(sigma) = 2.12(2.04)\%$. The term R_{psi} was defined previously by Cooper & Hawthorne (2018) as the agreement between absorption-corrected intensities of identical reflections measured several times at different positions around their diffraction vectors and represents a measure of the intrinsic reproducibility of measurement for the data collection. The combined unit-cell metrics and Laue merging of the X-ray intensity data does not clearly distinguish the correct symmetry as triclinic or monoclinic. However, the prominent reflections that violate both the presence of a 2_1-screw axis and an a-glide plane suggest that the correct symmetry cannot be monoclinic, as $P2_1$ and Pa are the only valid choices for subgroup symmetry that are compatible with the structure topology. In considering the two triclinic possibilities, we note that the distinction between $P1$ and $P\overline{1}$ symmetry (in relation to merging of Freidel pairs) is not overwhelming, as R_{psi} for $P1$ (2.12%) is only slightly lower than R_{merge} for $P\overline{1}$ (2.61%). The E-statistic result of $|E^2 - 1| = 0.783$ favors an acentric space group (*i.e.*, $P1$).

Confirmation of P1 symmetry

Our decision to accept $P1$ as the correct symmetry for the 'Ca-hingganite-(Y)' structure model, after testing refinement models in space groups $P2_1/a$, $P\overline{1}$, and $P1$, is based upon two factors: (1) the observed order of the A-site cations and (2) the final R_1 value. Allowance for possible twinning was incorporated into the refinement models. As we had recently recorded significant order of A-site cations in 'minasgeraisite-(Y)' compatible with $P1$ symmetry, we began refinement of the 'Ca-hingganite-(Y)' structure model in $P1$ using the structure model of 'minasgeraisite-(Y)' as a guide (Cooper & Hawthorne 2018). Our 'Ca-hingganite-(Y)' $P1$ structure model has three distinct scattering magnitudes over four A sites that can only be consistent with $P1$ symmetry. Additionally, the lowest R_1 value occurs for the $P1$ refinement. We conclude that the correct symmetry for 'Ca-hingganite-(Y)' is $P1$ and summarize our refinement observations in $P2_1/a$ and $P1$ below, as they may help to guide other investigators in the pursuit of possible lower symmetry in minerals of the gadolinite supergroup.

$P2_1/a$ refinement

Using the starting model of Miyawaki *et al*. (2007), we were able to refine a reasonably well-behaved anisotropic-displacement model to $R_1 = 12.85\%$. As noted earlier, there were numerous reflections observed that are in violation of a 2_1-screw axis and a-glide plane; however, these reflections do not contribute to the $P2_1/a$ refinement result, as they are removed by the refinement software. This initial refinement contained many reflections with $|F_o| > |F_c|$ in the worst-fit reflection list, suggesting that twinning may be present. Inclusion of a refining (100) twin-component lowered the R_1 value to 4.64% with a refined twin-fraction of 0.371(5). This fully anisotropic model contains variable refining site-scattering at the A, M, and Q cation sites, with assigned scattering factors ($A = Y$, $M = Fe$, $T = Si$, $Q = Be$). As such, there are no additional degrees of freedom that we can give the model to allow for further possible reduction in the observed R_1 value. The list of worst-fit reflections still contains all reflections with $|F_o| > |F_c|$, but they are now in closer relative agreement. On its own, this refinement model in $P2_1/a$ seems quite reasonable, and one might incorrectly accept it as is and attribute the slightly higher R value to less-than-ideal single-crystal quality or perhaps "twinning issues". However, one must not forget that the observed reflections violating the space group have also been ignored in this $P2_1/a$ refinement; if they were included, R would be significantly higher.

Initial P1 refinement

We adopted the $P1$ structure model used for 'minasgeraisite-(Y)', in which all general sites in

$P2_1/a$ split into four non-equivalent sites (Cooper & Hawthorne 2018), with the following assignment of scattering factors: $A = Y$, $M = Fe$, $T = Si$, $Q = Be$. All atom coordinates were allowed to refine independently. The site occupancies for all A and Q sites were refined independently and later assessed for relative scattering differences that might indicate significant cation order. As completely unrestrained refinement of all coordinates *and* cation site-occupancies *and* displacement parameters can result in correlated drift of the refined parameters in structures with strong pseudosymmetry, we coupled the refining isotropic-displacement parameters for all sites equivalent in $P2_1/a$ symmetry (*e.g.*, all four A sites had the same refining U_{iso} value). This refinement strategy produced meaningful isotropic-displacement parameters at all sites and allowed us to robustly test for significant site-scattering differences among the individual A and M sites. This model converged well and refined to $R_1 = 10.20\%$. It was immediately apparent that the four A sites contained significant differences in their refined site-scattering values [$A1 = 44.9(5)$, $A2 = 19.2(3)$, $A3 = 27.6(5)$, and $A4 = 32.7(4)$ eps (electrons per site)]. As the chemical analysis (Table 1) shows that ^{39}Y and ^{20}Ca are the dominant A site cations, it is immediately apparent that there is significant Ca–Y order over the A sites. Additionally, there are three distinctive A site-scattering signatures (heavy: ~45, light: ~19, and intermediate: ~30 eps), which collectively can only be consistent with $P1$ symmetry.

Twin P1 refinement

Next, we introduced a refining (100) twin-component that reduced the R_1 value to 3.67%, with a reported twin-fraction of 0.3614(18). The site-scattering values at the four A sites refined to the following values: $A1 = 40.76(16)$, $A2 = 20.67(12)$, $A3 = 28.94(12)$, and $A4 = 30.62(12)$ eps. Although these site-scattering values differ from those in the previous untwinned $P1$ model by more than the standard deviations, the same distinctive differences in site-scattering among the A sites remained. The Flack parameter of 0.517(13) indicated the possibility of additional racemic (*i.e.*, inversion) twinning [$\bar{1}00/0\bar{1}0/00\bar{1}$], and so the refinement model was updated with the inclusion of two additional refining twin-components to manage racemic-twin fractions. This further reduced the R_1 value to 2.83% and the resulting primary-domain fraction, twin (100) fraction, and two respective racemic fractions are: 0.324, 0.165(6), 0.318(7), and 0.193(6). Thus, the crystal can be described as containing a primary domain (~1/3 volume) with a near-equal racemic-twin component (~1/3 volume) and a (100) twin-component (~1/6 volume) with an associated near-equal racemic component (~1/6 volume). Minor changes to the A site-scattering values gave $A1 = 40.18(12)$, $A2 = 20.05(8)$, $A3 = 29.17(8)$, and $A4 = 30.42(12)$ eps.

Fully independent P1 model

In the preceding refinement models, all site-scattering was modelled using restrained refining isotropic-displacement parameters, in which similar sites (*i.e.*, identical in a $P2_1/a$ model) were coupled (*i.e.*, all four A sites were constrained to have the same refining U_{iso} value). Additionally, all A sites were assigned the Y scattering-factor, where the refined site-scattering values (in conjunction with the chemistry) clearly indicated that varying Ca was also present. This early strategy provided stable and convergent refinements that allowed comparison between site-scattering values of the untwinned and twinned models. However, the $P1$ structure contains distinctive differences among its A sites with respect to refined site-scattering values and mean bond-lengths. Based on the magnitudes of the A site-scattering values, the following scattering-factor assignments were adopted: $A1 = Y$, $A2 = Ca$, $A3,A4 = Y,Ca$, with the site-occupancies of the $A1$ and $A2$ sites refining freely and the $A3$ and $A4$ site-occupancies allowed to refine in terms of relative Ca and Y contributions that sum to full occupancy of the sites. The A sites were then finally updated to include a fixed Ln content [based on the Ln content measured by electron-microprobe analysis (Table 1) and the assumption of complete Ln–Y disorder]; this procedure is discussed in more detail below. The A site-scattering results from the earlier and final refinement models are compared in Figure 2; it is significant that the distinctive site-scattering differences between the A sites exist irrespective of the details of the model pertaining to twinning or assignment of scattering factors. As the chemical composition shows that Fe is the dominant M cation, both M sites were assigned the Fe scattering-factor with independently refined occupancy factors. Slight variations in site-scattering values and mean bond-lengths were observed for the Q sites, and these tetrahedrally coordinated sites were progressively modelled in terms of coupled Be and Si site-occupancy refinement with fixed B content in a multi-step process further discussed below. We wanted to have the greatest freedom with respect to refinement of atomic displacements (*i.e.*, full independent anisotropic modelling), but we also wanted the refinement to avoid non-positive-definite displacement values. We were able to produce a well-behaved fully anisotropic-displacement model for all sites (except the lightest Q

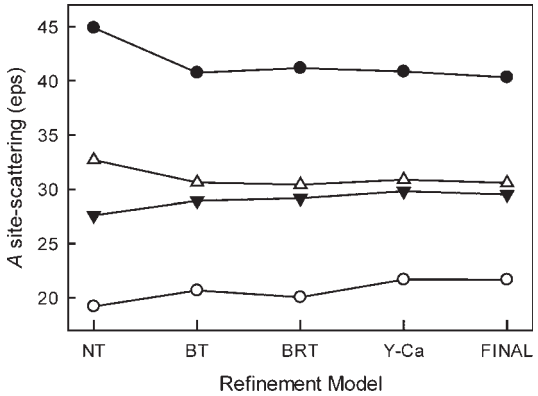

FIG. 2. Refined site-scattering values (eps) for the *A* sites in 'Ca-hingganite-(Y)' for various refinement models. NT: no twinning; BT: basic (100) twinning; BRT: basic + racemic twinning; Y–Ca: twin + (Y,Ca) scattering factors; FINAL: final twin model with Er–Y–Ca scattering factors. Standard deviations ≤ symbol size.

sites, which were refined with independent isotropic-displacement parameters). Our final twin-refinement model converged to $R_1 = 2.28\%$. Details pertaining to the refinement are given in Table 2, refined atom coordinates and displacement parameters are listed in Table 3, selected interatomic distances are given in Table 4, *Q*-site cation assignments are given in Table 5, and refined site-scattering values along with assigned site occupancies are given in Table 6.

*P*1 CRYSTAL STRUCTURE: CATION ASSIGNMENT AND ORDER

The Q sites

The four *Q* sites were assigned the Be scattering factor, and the site occupancies were allowed to refine unconstrained, giving 4.56(12), 5.36(16), 5.16(16), and 5.04(12) eps for the *Q*1, *Q*2, *Q*3, and *Q*4 sites, respectively. For all *Q* sites, the site scattering (Hawthorne *et al*. 1995) exceeds the ideal value of 4 eps for full occupancy by Be and suggests the presence of a heavier element, probably B (Demartin *et al*. 2001). Demartin *et al*. (2001) derived the following linear relation for the gadolinite-group minerals:

$$^{Q}\mathrm{B} = 1 - [(<Q\text{–}\mathrm{O}>_{\mathrm{O2,3,4}} - 1.475)/0.173]$$

where $<Q\text{–}\mathrm{O}>_{\mathrm{O2,3,4}}$ is derived from the bond lengths involving the three non-(OH) anions at O2, O3 and O4, and ^{Q}B is the content of tetrahedrally coordinated B. Applying this relation to 'Ca-hingganite-(Y)' gives the following compositions for the *Q* sites: $^{Q1}(\mathrm{Be}_{0.62}\mathrm{B}_{0.38})$, $^{Q2}(\mathrm{Be}_{0.58}\mathrm{B}_{0.42})$, $^{Q3}(\mathrm{Be}_{0.66}\mathrm{B}_{0.34})$, and $^{Q4}(\mathrm{Be}_{0.55}\mathrm{B}_{0.45})$. Thus, the observed site-scattering and mean bond-length information is consistent with significant B occupancy of the *Q* sites. As ^{4}Be and ^{5}B have similar scattering factors, coupled site-occupancy refinement of B and Be is not the best refinement strategy. Of all the cations that are possible *Q*-site constituents (Be, B, Al, Si), we can rule out Al, as it was below detection limit in the electron-microprobe analysis. As Si has an effective ionic radius (0.26 Å) that is nearly the same as Be (0.27 Å), Si will proxy for Be in terms of size; tetrahedrally coordinated B has a distinctly different radius (0.11 Å), and the B content can be reliably inferred from the $<Q\text{–}\mathrm{O}>_{\mathrm{O2,3,4}}$ distances (Demartin *et al*. 2001). Any Si present can subsequently be detected from the relative excess scattering, as Si (14 e) is a considerably stronger scattering species than Be (4 e). We inserted a fixed B content at each *Q* site that was calculated from the $<Q\text{–}\mathrm{O}>$ – Be/(B + Be) relation of Demartin *et al*. (2001) and refined the remaining site-scattering using the Be scattering factor. At the end of this stage of the refinement, this refined Be occupancy was assessed; if the refined Be occupancy exceeded (1 – fixed B occupancy), the site was inferred to have Si present (*i.e*., the observed site-scattering is in excess of coupled [B + Be] full occupancy). Excess scattering was observed for each *Q* site, and the refinement model was updated to include refining Si and Be occupancies that were mutually coupled to the (1 – fixed B) occupancy for each *Q* site. The $<Q\text{–}\mathrm{O}>_{\mathrm{O2,3,4}}$ distances were monitored throughout, and any change in these values resulted in an update of the fixed B content according to the $<Q\text{–}\mathrm{O}>$ – Be/(B + Be) relation of Demartin *et al*. (2001). In Table 5, we give the bond-lengths, site-scattering, and site-assignment details for the *Q* sites. The combined *Q*-site composition, developed from the site-scattering and mean bond-lengths for the present crystal, in conjunction with the application of the $<Q\text{–}\mathrm{O}>$ – Be/(B + Be) relation of Demartin *et al*. (2001), is $(\mathrm{Be}_{2.24}\mathrm{B}_{1.58}\mathrm{Si}_{0.18})_{\Sigma 4.00}$.

The T sites

The $<T\text{–}\mathrm{O}>$ distances range from 1.630 to 1.636 Å for the crystal of 'Ca-hingganite-(Y)' (Table 4) and are consistent with complete occupancy by Si (Demartin *et al*. 2001); additionally, there was no significant departure from full Si occupancy in the refinement. The combined *T*-site composition is $\mathrm{Si}_{4.00}$.

The (Q +T) site composition

Combining our *Q*- and *T*-site assignments gives $(\mathrm{Si}_{4.18}\mathrm{Be}_{2.24}\mathrm{B}_{1.58})_{\Sigma 8.00}$, and the chemical data were normalized using this crystal-chemically derived Be and B content (Table 1).

TABLE 3. ATOM COORDINATES AND DISPLACEMENT PARAMETERS FOR 'Ca-HINGGANITE-(Y)'

Atom	*x/a*	*y/b*	*z/c*	U_{11}	U_{22}	U_{33}	U_{23}	U_{13}	U_{12}	U_{eq} / U_{iso}
*A*1	0.3337(3)	0.1072(3)	0.0022(5)	0.00919(18)	0.00808(18)	0.00807(18)	0.00029(13)	0.0018(3)	–0.0019(3)	0.00845(12)
*A*2	–0.3332(3)	–0.1061(4)	–0.0028(6)	0.0094(4)	0.0118(5)	0.0111(5)	–0.0000(3)	0.0001(5)	–0.0015(5)	0.0108(3)
*A*3	0.1684(3)	0.6079(4)	–0.0028(5)	0.0095(3)	0.0093(4)	0.0084(3)	–0.00056(19)	0.0006(4)	–0.0002(5)	0.00905(19)
*A*4	0.8345(3)	0.3964(3)	0.0019(5)	0.0091(3)	0.0095(3)	0.0082(3)	–0.00013(18)	0.0015(4)	–0.0014(4)	0.00895(17)
*M*1	0	0	0	0.0110(8)	0.0114(9)	0.0073(7)	0.0002(5)	0.0028(5)	–0.0005(6)	0.0099(5)
*M*3	0.5004(3)	0.5044(6)	–0.0006(7)	0.0075(8)	0.0076(9)	0.0081(7)	–0.0009(5)	0.0030(5)	–0.0011(6)	0.0077(5)
*Q*1	0.3387(9)	0.4134(8)	0.4437(13)							0.0090(16)
*Q*2	–0.3367(7)	–0.4113(8)	–0.4531(13)							0.0092(16)
*Q*3	0.1650(8)	0.9148(9)	–0.4419(14)							0.0149(18)
*Q*4	0.8394(8)	0.0897(7)	0.4528(11)							0.0061(13)
*T*1	0.0826(3)	0.2737(4)	0.5227(6)	0.0078(6)	0.0085(8)	0.0075(8)	0.0015(6)	0.0004(6)	–0.0024(6)	0.0079(3)
*T*2	–0.0793(3)	–0.2717(4)	–0.5225(6)	0.0093(6)	0.0078(7)	0.0087(8)	–0.0017(6)	–0.0001(6)	–0.0007(6)	0.0086(3)
*T*3	0.4190(3)	0.7748(4)	–0.5222(6)	0.0078(6)	0.0086(7)	0.0065(7)	0.0004(6)	–0.0014(6)	–0.0006(6)	0.0076(3)
*T*4	0.5816(3)	0.2295(4)	0.5228(6)	0.0106(7)	0.0085(8)	0.0082(8)	–0.0004(6)	0.0016(6)	0.0012(7)	0.0091(4)
O11	0.0346(6)	0.4142(8)	0.7527(11)	0.013(2)	0.010(2)	0.006(2)	–0.0039(16)	0.0027(16)	0.0002(18)	0.0095(10)
O12	–0.0316(7)	–0.4038(10)	–0.7670(14)	0.020(3)	0.019(2)	0.011(2)	–0.0008(19)	–0.0022(19)	0.000(2)	0.0166(11)
O13	0.4636(6)	0.9140(9)	–0.7562(12)	0.014(2)	0.017(2)	0.005(2)	0.0046(17)	–0.0023(16)	0.0043(18)	0.0122(10)
O14	0.5295(6)	0.0963(8)	0.7596(13)	0.0092(19)	0.0083(19)	0.012(2)	–0.0029(17)	0.0016(16)	0.0001(15)	0.0099(10)
O21	0.4559(5)	0.2933(7)	0.3174(12)	0.0072(18)	0.0113(19)	0.014(2)	0.0013(16)	–0.0009(16)	–0.0005(15)	0.0109(9)
O22	–0.4504(5)	–0.2895(7)	–0.3335(11)	0.016(2)	0.0101(18)	0.013(2)	–0.0033(15)	–0.0073(17)	0.0037(16)	0.0131(8)
O23	0.0474(5)	0.7947(7)	–0.3217(12)	0.0105(18)	0.0061(17)	0.0116(19)	–0.0020(15)	–0.0037(15)	0.0020(15)	0.0094(8)
O24	0.9554(6)	0.2103(7)	0.3275(13)	0.016(2)	0.013(2)	0.016(2)	0.0037(18)	–0.0074(17)	–0.0052(18)	0.0151(10)
O31	0.2031(6)	0.3401(7)	0.3090(12)	0.017(2)	0.011(2)	0.013(2)	0.0009(16)	0.0059(16)	–0.0027(16)	0.0135(10)
O32	–0.1990(5)	–0.3427(7)	–0.3166(11)	0.007(2)	0.020(2)	0.0102(18)	0.0011(16)	–0.0003(13)	0.0003(15)	0.0124(9)
O33	0.3024(5)	0.8437(7)	–0.3030(11)	0.0045(19)	0.0157(19)	0.0150(19)	0.0004(16)	0.0053(13)	0.0011(14)	0.0117(9)
O34	0.7044(6)	0.1595(7)	0.3208(12)	0.021(2)	0.014(2)	0.0088(18)	–0.0048(15)	–0.0032(15)	0.0065(18)	0.0148(9)
O41	0.1456(6)	0.1042(8)	0.6911(12)	0.017(3)	0.010(2)	0.012(2)	0.0063(16)	–0.0063(17)	–0.0003(18)	0.0127(10)
O42	–0.1430(5)	–0.0966(7)	–0.6821(10)	0.011(2)	0.0124(17)	0.0137(18)	0.0006(15)	–0.0013(15)	0.0050(16)	0.0124(9)
O43	0.3553(6)	0.6035(7)	–0.6855(12)	0.011(2)	0.0087(18)	0.020(2)	–0.0030(16)	–0.0066(17)	–0.0027(16)	0.0130(10)
O44	0.6447(6)	0.4032(8)	0.6849(12)	0.014(2)	0.014(2)	0.011(2)	–0.0057(17)	–0.0003(17)	0.0021(17)	0.0132(10)
φ1	0.3368(7)	0.4095(7)	0.7759(10)	0.0080(17)	0.0153(16)	0.0111(16)	0.0000(14)	–0.001(2)	–0.005(2)	0.0115(8)
φ2	–0.3317(7)	–0.4148(8)	–0.7762(12)	0.019(2)	0.015(2)	0.0076(19)	–0.0020(17)	0.001(2)	0.003(2)	0.0139(10)
φ3	0.1686(6)	0.9158(8)	–0.7752(11)	0.0104(19)	0.0114(18)	0.0104(19)	0.0005(16)	–0.0021(18)	0.0022(19)	0.0107(9)
φ4	0.8375(8)	0.0916(7)	0.7768(11)	0.0117(18)	0.0169(18)	0.0105(16)	–0.0006(15)	0.005(2)	–0.002(2)	0.0131(8)

TABLE 4. SELECTED INTERATOMIC DISTANCES (Å) FOR 'Ca-HINGGANITE-(Y)'

*A*1–O13	2.262(6)	*A*2–O13	2.329(6)	*A*3–O11	2.294(5)	*A*4–O11	2.308(5)
*A*1–O14	2.253(6)	*A*2–O14	2.340(6)	*A*3–O12	2.272(6)	*A*4–O12	2.293(7)
*A*1–O21	2.388(5)	*A*2–O22	2.399(5)	*A*3–O23	2.397(5)	*A*4–O24	2.413(5)
*A*1–O31	2.633(5)	*A*2–O32	2.689(5)	*A*3–O31	2.543(5)	*A*4–O32	2.518(5)
*A*1–O33	2.494(5)	*A*2–O34	2.567(5)	*A*3–O33	2.647(4)	*A*4–O34	2.683(5)
*A*1–O41	2.373(5)	*A*2–O42	2.419(5)	*A*3–O43	2.383(5)	*A*4–O44	2.404(5)
*A*1–φ1	2.539(5)	*A*2–φ2	2.583(6)	*A*3–φ1	2.480(6)	*A*4–φ2	2.423(6)
*A*1–φ3	2.428(5)	*A*2–φ4	2.489(6)	*A*3–φ3	2.579(5)	*A*4–φ4	2.553(5)
<*A*1–O>	2.421	<*A*2–O>	2.477	<*A*3–O>	2.449	<*A*4–O>	2.449
*M*1–O23	2.237(5)			*M*3–O21	2.250(5)		
*M*1–O24	2.277(6)			*M*3–O22	2.282(6)		
*M*1–O41	2.204(6)			*M*3–O43	2.207(6)		
*M*1–O42	2.197(5)			*M*3–O44	2.207(6)		
*M*1–φ3	2.078(6)			*M*3–φ1	2.062(6)		
*M*1–φ4	2.045(7)			*M*3–φ2	2.063(7)		
<*M*1–O>	2.173			<*M*3–O>	2.179		
*Q*1–O21	1.592(9)	*Q*2–O22	1.562(8)	*Q*3–O23	1.584(8)	*Q*4–O24	1.584(8)
*Q*1–O31	1.584(10)	*Q*2–O32	1.593(8)	*Q*3–O33	1.601(9)	*Q*4–O34	1.565(9)
*Q*1–O43	1.579(7)	*Q*2–O44	1.567(7)	*Q*3–O41	1.585(8)	*Q*4–O42	1.565(6)
*Q*1–φ1	1.582(6)	*Q*2–φ2	1.540(7)	*Q*3–φ3	1.587(7)	*Q*4–φ4	1.543(6)
<*Q*1–O>	1.584	<*Q*2–O>	1.566	<*Q*3–O>	1.589	<*Q*4–O>	1.564
*T*1–O11	1.602(5)	*T*2–O12	1.609(7)	*T*3–O13	1.599(6)	*T*4–O14	1.601(6)
*T*1–O24	1.633(5)	*T*2–O23	1.651(5)	*T*3–O22	1.644(5)	*T*4–O21	1.651(5)
*T*1–O31	1.645(5)	*T*2–O32	1.627(5)	*T*3–O33	1.640(4)	*T*4–O34	1.637(5)
*T*1–O41	1.640(6)	*T*2–O42	1.656(5)	*T*3–O43	1.641(5)	*T*4–O44	1.651(6)
<*T*1–O>	1.630	<*T*2–O>	1.636	<*T*3–O>	1.631	<*T*4–O>	1.635

The M sites

The *M*-site composition from the empirical formula (20 oxygen basis) is $(Fe_{0.794}Mn_{0.009}Mg_{0.006}\square_{1.191})_{\Sigma 2.00}$ and gives a combined calculated electron-scattering of 20.94 *epfu* (electrons per formula unit). This is in good agreement with the combined observed site-scattering values at the *M*1 and *M*3 sites: 10.53(10) + 9.85(10) = 20.38 *epfu*. In agreement with the findings of Cooper & Hawthorne (2018) on 'minasgeraisite-(Y)', there is no significant Ca at the *M* site(s) in our 'Ca-hingganite-(Y)' crystal. The site-scattering values for our 'Ca-hingganite-(Y)' refinement indicate that the dominant constituent at both the *M*1 and *M*3 sites must be vacancy. The observed <*M*1–O> and <*M*3–O> distances of 2.173 and 2.179 Å, respectively, agree with the range (2.174–2.200 Å) reported for other gadolinite-group minerals with variable Fe-occupancy at the *M* site (Demartin *et al*. 2001). The (OH) content at the φ site(s), calculated from the vacancy content at

TABLE 5. *Q*-SITE CATION ASSIGNMENTS FOR 'Ca-HINGGANITE-(Y)'

	*Q*1	*Q*2	*Q*3	*Q*4
$<Q–O_{2^*,3^*,4^*}>$	1.585	1.574	1.590	1.571
Be[1]	0.64	0.57	0.66	0.55
B[1]	0.36	0.43	0.34	0.45
inferred scattering (eps)	4.36	4.43	4.34	4.45
Observed scattering (eps) [fixed B, refining Be/Si occupancy]	4.56(12)	5.01(16)	4.94(16)	4.88(12)
Be	0.62	0.51	0.60	0.51
B	0.36	0.43	0.34	0.45
Si	0.02	0.06	0.06	0.04

[1] $^{Q}B = 1 - [(<Q–O>_{O2,3,4} - 1.475)/0.173]$, $^{Q}Be = (1 - {}^{Q}B)$; Demartin *et al.* (2001).

TABLE 6. FINAL SITE-SCATTERING VALUES AND ASSIGNED SITE OCCUPANCIES FOR 'Ca-HINGGANITE-(Y)'

	eps	^{20}Ca	^{39}Y	^{68}Er	□	^{26}Fe	^{4}Be	^{5}B	^{14}Si
*A*1	40.33(12)	0.031(6)	0.903(6)	[0.066]					
*A*2	21.67(12)	0.920(6)	0.075(6)	[0.005]					
*A*3	29.50(8)	0.546(6)	0.424(6)	[0.030]					
*A*4	30.58(8)	0.495(6)	0.471(6)	[0.034]					
Σ	122.08	1.992	1.873	0.135					
*M*1	10.53(10)				0.595	0.405(4)			
*M*3	9.85(10)				0.621	0.379(4)			
Σ	20.38				1.216	0.784			
*Q*1	4.56(12)						0.621(9)	[0.36]	0.020(9)
*Q*2	5.01(16)						0.512(10)	[0.43]	0.058(10)
*Q*3	4.94(16)						0.601(11)	[0.34]	0.059(11)
*Q*4	4.88(12)						0.507(8)	[0.45]	0.043(8)
Σ							2.24	1.58	0.18
*T*1									[1.00]
*T*2									[1.00]
*T*3									[1.00]
*T*4									[1.00]
Σ									4.00

[ ] denotes fixed occupancy.

M using the assumption that 2(OH) groups correspond to each 'vacancy' at the *M* site(s) (Demartin *et al.* 2001), gives a calculated φ-site composition of $[(OH)_{2.382}O_{1.618}]_{\Sigma 4.00}$ *pfu* for our 'Ca-hingganite-(Y)' crystal; our crystal is therefore (OH)-dominant at the φ site(s).

The A sites

Our chemical results from electron-microprobe analysis show that the four [8]-coordinated *A* sites are expected to contain mainly Ca and Y, along with minor lanthanides (relative HREE enrichment), where the Ca : (Y + Ln) ratio is close to 1:1 (Table 1). As Y^{3+} and Ln^{3+} have the same charge and similar size, we assumed that they will be completely disordered. Moreover, as the Ln content is quite small (*i.e.*, Ln / (Ln + Y) ≈ 0.068), we initially modelled the site-scattering at the *A* sites using only Y (in addition to the Ca scattering factor). Our *P*1 refinement model in all cases (*i.e.*, no twinning, basic twinning, basic + racemic twinning, Y–Ca partitioned *A*-site scattering assignment) produced three distinct site-scattering signatures over the four *A* sites (*A*1 = heavy; *A*2 = light; *A*3,*A*4 = intermediate). The site-scattering results for the four *A* sites are plotted for each of the refinement models in Figure 2. It is clear that the following cation order occurs over the *A* sites, irrespective of refinement strategy: *A*1 = Y, *A*2 = Ca, *A*3, *A*4 = Ca, Y. Our twin-refinement model, using these scattering-factor assignments, gives *A*-site scattering-values of *A*1 = 40.87(12), *A*2 = 21.68(12), *A*3 = 29.80(8), and *A*4 = 30.87(8) eps. As three of the four *A* sites contain significant Y, we expect that approximately 7% of the trivalent-cation occupancy at these sites is comprised of Ln elements (HREE enriched, ^{70}Yb dominant, with a mean scattering signature of ^{68}Er). The three principal scattering-species, ^{20}Ca, ^{39}Y, and ^{68}Er, involve quite different scattering factors, therefore the most accurate refined site-scattering results can only be obtained by inclusion of all three scattering factors, thus the need to include minor Ln occupancy at the *A* sites. Because a refining site-occupancy can be expressed only in terms of coupled binary scattering-factors (Hawthorne 1983), we elected to approximate a Ln content for each of the *A* sites and then fix this Ln occupancy, allowing coupled Ca–Y site-occupancy refinement to account for the remaining site-scattering, as is commonly done for occupancy of a site by many cations in minerals. This Ln approximation was developed in the following manner: first we assumed that trivalent cations at the *A* sites are 93.2% ^{39}Y and 6.8% ^{68}Er and that their combined presence could be approximated by an averaged scattering entity ($^{40.97}$Y*); the current observed scattering values (*i.e.*, *A*1 = 40.87, *A*2 = 21.68, *A*3 = 29.80, *A*4 = 30.87 eps: electrons per site) can thus be expressed in terms of ^{20}Ca and $^{40.97}$Y* to give $A1 = Y^*_{0.995}Ca_{0.005}$, $A2 = Y^*_{0.080}Ca_{0.920}$, $A3 = Y^*_{0.467}Ca_{0.533}$, and $A4 = Y^*_{0.518}Ca_{0.482}$; and the ^{68}Er fixed occupancy values are: $^{W1}Er_{0.068}$, $^{W2}Er_{0.005}$,

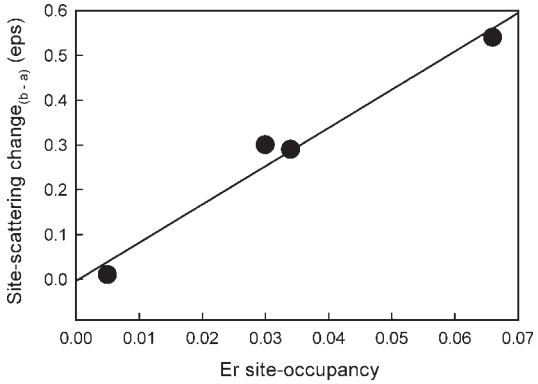

FIG. 3. Relative change (before – after) in observed site-scattering values (eps) at the *A* sites in 'Ca-hingganite-(Y)' *versus* the fixed Er site-occupancy.

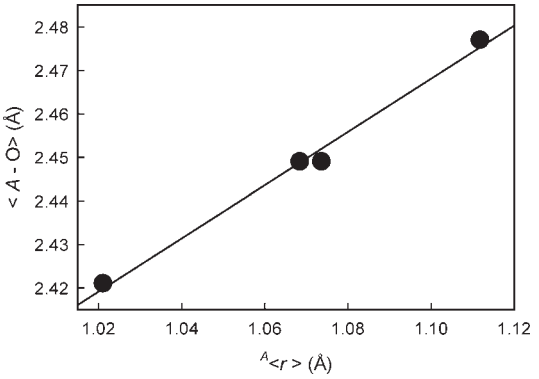

FIG. 4. The constituent radii ($^{A}\langle r\rangle$) calculated from the Er–Y–Ca site-occupancies at the *A* sites in 'Ca-hingganite-(Y)' *versus* the observed <*A*–O> distances.

$^{W3}Er_{0.032}$, and $^{W4}Er_{0.035}$. The remaining scattering at each *A* site was then allowed to refine freely with coupled Ca and Y scattering factors. This produced updated total scattering values for each of the *A* sites, and the procedure was repeated until there was no change in the total scattering at each *A* site. The final site-scattering values obtained *via* inclusion of the Er, Y, and Ca scattering factors are: *A*1, 40.33 ($Er_{0.066}Y_{0.903}Ca_{0.031}$); *A*2, 21.67 ($Er_{0.005}Y_{0.075}Ca_{0.920}$); *A*3, 29.50 ($Er_{0.030}Y_{0.424}Ca_{0.546}$); and *A*4, 30.58 eps ($Er_{0.034}Y_{0.471}Ca_{0.495}$). To show the net effect on the observed site-scattering at the *A* sites in relation to the inclusion of the relatively minor ^{68}Er scattering contribution, we have plotted the difference in observed site-scattering (before ^{68}Er inclusion – after ^{68}Er inclusion) as a function of the fixed Er occupancy in Figure 3. There is a well-developed positive correlation between increasing assigned Er content and decreasing observed scattering at the site (*i.e.*, the *A*1 site with assigned $Er_{0.066}$ experiences a decrease in observed scattering of 0.54 eps relative to not including an Er component). The effective ionic radii, C.N. = [8], for the *A*-site cations are $Er^{3+} = 1.004$, $Y^{3+} = 1.019$, and $Ca^{2+} = 1.12$ Å (Shannon 1976). It was noted by Demartin *et al.* (2001) that the observed range for <*A*–O> of 2.420–2.438 Å for various gadolinite-group minerals does not show a reasonable bond-length variation with respect to Ca content. We plotted our observed <*A*–O> distances against the constituent radii ($^{A}\langle r\rangle$) calculated from our (Er–Y–Ca) content *via* site-scattering observations [*A*1 = ($Er_{0.066}Y_{0.903}Ca_{0.031}$) with $\langle r\rangle = 1.021$; *A*2 = ($Er_{0.005}Y_{0.075}Ca_{0.920}$) with $\langle r\rangle = 1.112$; *A*3 = ($Er_{0.030}Y_{0.424}Ca_{0.546}$) with $\langle r\rangle = 1.074$; and *A*4 = ($Er_{0.034}Y_{0.471}Ca_{0.495}$) with $\langle r\rangle = 1.068$ Å] (Fig. 4). Although the observed range in <*A*–O> is rather small (0.056 Å), its variation with respect to the calculated constituent radii calculated from the site-scattering results gives a very good linear correlation; this agreement serves to further validate the *P*1 structure model in terms of reported *A*-site cation order that is coupled to minor adjustments in *A*–O distances.

THE CHEMICAL FORMULA OF 'CA-HINGGANITE-(Y)'

As the single crystal used for the collection of the X-ray diffraction data was subsequently analyzed by electron-microbe analysis, we expect a high degree of conformity between the site-scattering results (SREF) and the chemical composition (EMPA), especially considering that the 10 random-point chemical analyses show little chemical variation across the crystal. So, although we made no direct measure of the Be or H contents, the combined SREF-EMPA approach is expected to provide reliable values for these elements. The Be and B values derived from our *Q* site composition $(Be_{2.24}B_{1.58}Si_{0.18})_{\Sigma 4.00}$, along with the $(OH)_{2.382}$ value derived from an assessment of the *M*-site cations, were entered into the normalization (20 anion basis) of the chemical data (Table 1). The resulting site-specific empirical formula is $^{A}(Ca_{2.021}Y_{1.811}Ln_{0.133})_{\Sigma 3.965}{}^{M}(\square_{1.191}Fe_{0.794}Mn_{0.009}Mg_{0.006})_{\Sigma 2}{}^{Q}(Be_{2.24}B_{1.58}Si_{0.224})_{\Sigma 4.044}{}^{T}Si_4O_{16}\ {}^{\varphi}[(OH)_{2.382}O_{1.618}]_{\Sigma 4}$. The *A*-site cations give a calculated electron-scattering value of 120.12 e, which is in good agreement with the refined value of 123.22 e using the Er–Y–Ca combined site-scattering curves; the *M*-site cations give a calculated electron-scattering value of 20.94 e, which is in close agreement with the 20.38 e refined using the Fe scattering curve; and the *Q*-site cations give a calculated electron-scattering value of 20.00 e, which is in good agreement with the 19.38 e refined using the Be–B–Si combined site-scattering curves (Table 6). Our crystal contains near-equal amounts of Ca and trivalent cations at the *A* sites, and the *M* site sites are dominated by

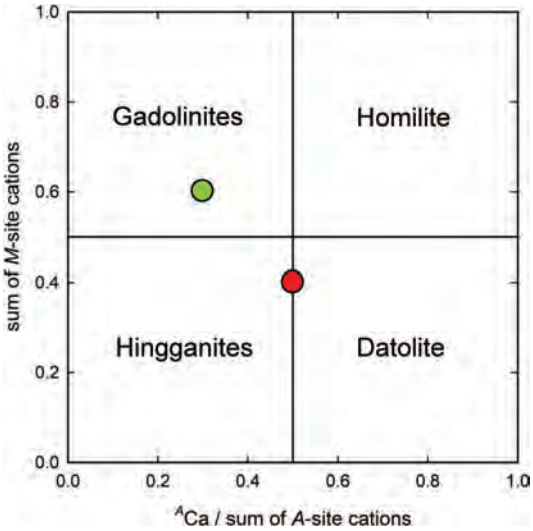

FIG. 5. Species classification diagram of the gadolinite group based on *M*- and *A*-site cations, reproduced from Bačík *et al.* (2017). Red circle = 'Ca-hingganite-(Y)' this study; green circle = 'minasgeraisite-(Y)' from Cooper & Hawthorne (2018).

vacancy. In the *M*- and *A*-site gadolinite-group classification diagram of Bačík *et al.* (2017), our crystal composition plots at the boundary of the hingganite and datolite fields (Fig. 5). Our *Q*-site composition has Be > B, and we therefore refer to our crystal as hingganite-(Y)-like. As the Ca content at the *A* sites approximates 50% total occupancy, the modified name 'Ca-hingganite-(Y)' seems most appropriate. The minor Si located at the *Q* site requires that an additional minor (~5%) constituent is needed to fully represent our crystal composition.

Triclinic Members of the Gadolinite Subgroup

Two minerals belonging to the gadolinite subgroup have now been identified as having significant *A*-site cation order consistent with (triclinic) *P*1 symmetry, namely 'minasgeraisite-(Y)' (Cooper & Hawthorne 2018) and 'Ca-hingganite-(Y)'. The single-crystal X-ray diffraction data for both minerals contain well-observed reflections that violate both the 2_1-screw axis and *a*-glide plane symmetry elements of (monoclinic) $P2_1/a$ symmetry. We note that a simulated X-ray powder pattern derived from our 'Ca-hingganite-(Y)' single-crystal X-ray intensity data shows only one well-resolved peak that violates the presence of an *a*-glide plane [3% relative intensity at 20.71° 2θ (Cu*K*α) belonging to the 101 and $\bar{1}01$ diffraction planes]. As shown for our 'Ca-hingganite-(Y)' crystal, a plausible but incorrect $P2_1/a$ refinement is easily produced *via* improper averaging of the truly triclinic data; therefore, the single-crystal X-ray intensity data must be carefully examined for observed reflections violating the space group $P2_1/a$. If these symmetry-violating reflections are observed, it is recommended that a simple (*i.e.*, restrained isotropic) *P*1 structure model is tested for the presence of any significant order of cations over the *A* sites. For the two *P*1 structures described ['Ca-hingganite-(Y)' and 'minasgeraisite-(Y)'], the lower symmetry is indicated by strong order of *A*-site cations and relatively minor order of cations at the *M*- and *Q*-sites. Any *A*-site cation order involving the relative order of high-contrast scattering species (*e.g.*, Ca *versus* Y,Ln) may be detected *via* accurate structure refinement. With regard to chemical composition, this is expected to be most applicable for intermediate members of the datolite (Ca) – gadolinite (Y,Ln) series. As twinning may be present, one must be careful of its correct management with respect to any structure model; however, based on the current work with 'Ca-hingganite-(Y)', significant *A*-site order can be readily distinguished prior to addressing the issue of twinning.

Acknowledgments

We thank Peter Bačík, an anonymous reviewer, and Associate Editor Jim Evans for their helpful remarks on this paper. This work was supported by a Discovery Grant from the Natural Sciences and Engineering Research Council of Canada to FCH and by Innovation Grants from the Canada Foundation for Innovation to FCH. We thank Mrs. Masako Shigeoka for her assistance with the electron-microprobe analysis and Harald Folvik, Natural History Museum, University of Oslo, for the scanning electron micrographs of 'Ca-hingganite-(Y)'.

References

Bačík, P., Fridrichová, J., Uher, P., Pršek, J., & Ondrejka, M. (2014) The crystal chemistry of gadolinite-datolite group silicates. *Canadian Mineralogist* **52**, 625–642.

Bačík, P., Miyawaki, R., Atencio, D., Cámara, F., & Fridrichová, J. (2017) Nomenclature of the gadolinite supergroup. *European Journal of Mineralogy* **29**, 1–16.

Cooper, M.A. & Hawthorne, F.C. (2018) Cation order in the crystal structure of 'minasgeraisite-(Y)'. *Mineralogical Magazine* **82**, 301–312.

Cooper, M.A., Hawthorne, F.C., Ball, N.A., Černý, P., & Kristiansen, R. (2006) Oftedalite, $(ScCa,Mn^{2+})_2KBe_3Si_{12}O_{30}$, a new mineral species of the milarite group from the Heftetjern pegmatite, Tørdal, Norway: Description

and crystal structure. *Canadian Mineralogist* **44**, 943–949.

Demartin, F., Minaglia, A., & Gramaccioli, C.M. (2001) Characterization of gadolinite-group minerals using crystallographic data only: the case of hingganite-(Y) from Cuasso al Monte, Italy. *Canadian Mineralogist* **39**, 1105–1114.

Foord, E.E., Gaines, R.V., Crock, J.G., Simmons, W.B., Jr., & Barbosa, C.P. (1986) Minasgeraisite, a new member of the gadolinite group from Minas Gerais, Brazil. *American Mineralogist* **71**, 603–607.

Hawthorne, F.C. (1983) Quantitative characterization of site occupancies in minerals. *American Mineralogist* **68**, 287–306.

Hawthorne, F.C., Ungaretti, L., & Oberti, R. (1995) Site populations in minerals: Terminology and presentation of results of crystal-structure refinement. *Canadian Mineralogist* **33**, 907–911.

Miyawaki, R., Matsubara, S., Yokoyama, K., & Okamoto, A. (2007) Hingganite-(Ce) and hingganite-(Y) from Tahara, Hirukawa-mura, Gifu Prefecture, Japan: The description on a new mineral species of the Ce-analogue of hingganite-(Y) with a refinement of the crystal structure of hingganite-(Y). *Journal of Mineralogical and Petrological Sciences* **102**, 1–7.

Miyawaki, R., Momma, K., Yokoyama, K., Shigeoka, M., Matsubara, S., Ito, M., Nakai, I., & Kristiansen, R. (2015) Mn-bearing hellandite-(Y) from the Heftetjern pegmatite, Tørdal, Norway. *Canadian Mineralogist* **53**, 345–356.

Miyawaki, R., Momma, K., Cooper, M.A., Hawthorne, F.C., & Kristiansen, R. (2018) Refinements of crystal structure of hingganite-(Y): Cation ordering and lowering symmetry. *Rare Earth Society of Japan Annual Meeting*.

Shannon, R.D. (1976) Revised effective ionic radii and systematic studies of interatomic distances in halides and chalcogenides. *Acta Crystallographica* **A32**, 751–767.

Sheldrick, G.M. (2008) A short history of *SHELX*. *Acta Crystallographica* **A64**, 112–122.

Received December 22, 2018. Revised manuscript accepted February 13, 2019.